Trajectory Tracking of a Fully-actuated Surface Vessel using Nonlinear Model Predictive Control

Leticia Mayumi Kinjo, Stefan Wirtensohn, Johannes Reuter, Tomas Menard, Olivier Gehan

Trajectory Tracking of a Fully-actuated Surface Vessel using Nonlinear Model Predictive Control

Leticia Mayumi Kinjo [*,**] **Stefan Wirtensohn** [**]
Johannes Reuter [**] **Tomas Menard** [*] **Olivier Gehan** [*]

[*] *LAC EA7478, ENSICAEN, 6 Bd du Marechal Juin, 14050 Caen Cedex, France (e-mail: {leticia.kinjo, tomas.menard, olivier.gehan}@ensicaen.fr).*
[**] *Institute of System Dynamics, University of Applied Sciences Konstanz, Konstanz, Germany (e-mail:{lkinjo, stwirten, jreuter}@htwg-konstanz.de)*

Abstract: The trajectory tracking problem for a fully-actuated real-scaled surface vessel is addressed in this paper. The unknown hydrodynamic and propulsion parameters of the vessel's dynamic model were identified using an experimental maneuver-based identification process. Then, a nonlinear model predictive control (NMPC) scheme is designed and the controller's performance is assessed through the variation of NMPC parameters and constraints tightening for tracking a curved trajectory.

Keywords: Fully-actuated autonomous surface vessels, nonlinear model predictive Control, trajectory tracking, parameter identification.

1. INTRODUCTION

Recently, the growth of worldwide interest in research and development of unmanned surface vessels (USV) has been encouraged by scientific, commercial, and military sectors to answer the increased demand for environmental monitoring, coastal defense, search and rescue activities, and transportation services (Liu et al. (2016)). For an autonomous surface vessel to perform such marine operations, it is crucial that it has a reliable control system capable of performing accurate maneuvers and tracking predefined reference trajectories. Hence, vessel motion control is an active field of research.

Many studies have proposed different design controllers to solve the trajectory tracking problem for USV, such as sliding-mode control Liu et al. (2015a), backstepping technique Dai et al. (2019), and adaptive control Wen et al. (2019). However, a major drawback of the aforementioned works is that the input or state constraints were not explicitly taken into account, which may lead to poor control performance or even actuator damages in real implementations. Model predictive control (MPC) is an efficient technique to overcome these shortcomings due to its capability of solving an optimal control problem in real-time and handling constraints directly. Therefore, it has been widely employed in vessel motion control problems.

In Yan and Wang (2012), a linear MPC (LMPC) combined with a recurrent neural network was used to solve the trajectory tracking problem for an underactuated vessel. In Zheng et al. (2014), a comparison between the performance of nonlinear MPC (NMPC) and linear MPC was made for a fully-actuated vessel, showing that NMPC was more accurate, even though it was costly in computational time. Illustrating the importance of choosing the solver for the optimization problem. NMPC was also implemented in Liu et al. (2015b) for an underactuated vessel with input and state constraints, evaluating its performance with and without environmental disturbances.

While in Lutz and Meurer (2021), LMPC is used to solve a trajectory planning and tracking for an underactuated vessel taking into account static and dynamic obstacles and input constraints, in Hagen et al. (2018), MPC is applied in a collision avoidance system, being responsible for choosing the optimal maneuver to bypass obstacles. In Abdelaal and Hahn (2016), the same problem is addressed using inequality constraints in the NMPC problem, which follow the International Regulations for Preventing Collisions at Sea COLREGS (1972). In Wang et al. (2018), an over-actuated robot tracks its pose using NMPC, performing experimental tests. Later, in Wang et al. (2020), a large-scaled over-actuated vessel realizes the trajectory tracking using a state and input constrained NMPC combined with a nonlinear moving horizon estimation (NMHE) to provide the state estimated values.

These previous controllers have considered the forces and moments of the vessel as inputs. However, for practical applications, these values might be difficult to measure. Furthermore, for real-scaled vessels, it is relevant to take into account the dynamic model of the propulsion system to obtain a more reliable model. Although all previous contributions have provided meaningful results using NMPC, there were not deep studies of the controller's performance regarding the tuning of parameters and constraints

tightening, which could give a better understanding of its calibration.

Fig. 1. Research boat Solgenia from the University of Applied Sciences Konstanz.

In this paper, the trajectory tracking problem is addressed for the real-scaled surface vessel from the University of Applied Sciences Konstanz called Solgenia, shown in Figure 1. First, the parameters of its dynamic model were identified using experimental data. Then, a NMPC problem with input and state constraints is formulated, considering not only the dynamic model of the vessel, but also the dynamic model of the thrusters. This is considered the main contribution of this paper. Besides that, the impact of the NMPC parameters and constraints tightening is assessed through simulation results to systematically analyze the controller's performance.

This paper is structured as follows. Section 2 provides a description of vessel's dynamics and its propulsion system, and it also presents a description of the parameter identification method. In Section 3, the trajectory tracking problem is formulated as a NMPC problem. The study of the controller's performance is given in Section 4. Section 5 concludes the paper and gives some perspectives of future work.

2. VESSEL DYNAMICS

2.1 Vessel Dynamic Model

Vessels experience motion in 6 degrees of freedom (DOF) as illustrated in Figure 2. Two coordinate frames are usually defined: the North-East-Down (NED) frame $e = (x_e, y_e, z_e)$, which can be considered as the inertial frame, and the body-fixed frame $b = (x_b, y_b, z_b)$, which is fixed on the vessel and is, therefore, a moving reference frame.

For a horizontal motion of a surface vessel, the 3 DOF model of its dynamics is conventionally represented as in Fossen (2011):

$$\dot{\boldsymbol{\eta}} = \boldsymbol{R}(\psi)\boldsymbol{\nu} \tag{1}$$

$$\boldsymbol{M}\dot{\boldsymbol{\nu}} + \boldsymbol{C}_{RB}(\boldsymbol{\nu})\boldsymbol{\nu} + \boldsymbol{N}(\boldsymbol{\nu})\boldsymbol{\nu} = \boldsymbol{\tau}(n_{AT}, \alpha, n_{BT}) \tag{2}$$

where $\boldsymbol{\eta} = [x, y, \psi]^T$ denotes the position and orientation angle of the vessel in the NED frame, while $\boldsymbol{\nu} = [u, v, r]^T$ represents the vessel's velocities in the body-fixed frame. The research boat Solgenia has a propulsion system formed by an azimuth thruster at the back and a bow thruster at the front as shown in Figure 2. Therefore, $\boldsymbol{\tau}(n_{AT}, \alpha, n_{BT})$ represents the control forces and moments acting on the vessel, which depend on the angle α and velocity n_{AT} of the azimuth thruster and the velocity n_{BT} of the bow thruster. The kinematic Eq. (1) describes the conversion of the velocities from the body-fixed to the NED frame through the transformation matrix $\boldsymbol{R}(\psi)$ given by:

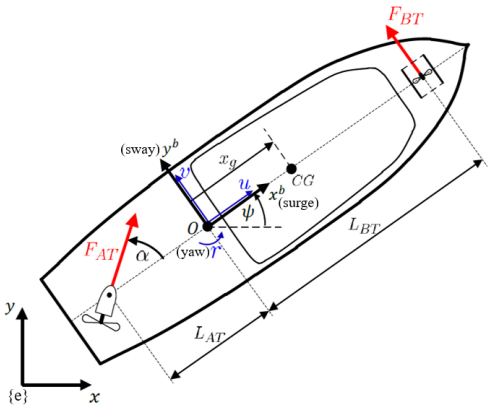

Fig. 2. Coordinate systems and actuators configuration of Solgenia

$$\mathbf{R}(\psi) = \begin{pmatrix} cos(\psi) & -sin(\psi) & 0 \\ sin(\psi) & cos(\psi) & 0 \\ 0 & 0 & 1 \end{pmatrix} \tag{3}$$

In Eq. (2), $\boldsymbol{M}$ is the positive-definite symmetric added mass summed with the vessel's mass, $\boldsymbol{C}_{RB}(\boldsymbol{\nu})$ is the skew-symmetric Coriolis and centripetal matrix. They can be written as:

$$\mathbf{M} = \begin{pmatrix} m - X_{\dot{u}} & 0 & 0 \\ 0 & m - Y_{\dot{v}} & mx_g - Y_{\dot{r}} \\ 0 & mx_g - N_{\dot{v}} & J_{comb} \end{pmatrix} \tag{4}$$

$$\boldsymbol{C}_{RB} = \begin{pmatrix} 0 & -mr & -mx_g r \\ mr & 0 & 0 \\ mx_g r & 0 & 0 \end{pmatrix} \tag{5}$$

where m is the vessel's mass, x_g is the displacement of the center of gravity (CG) in x-direction, $X_{\dot{u}}$ is the added mass in x^b-direction, $Y_{\dot{v}}$ is the added mass in y^b-direction, $Y_{\dot{r}}$ and $N_{\dot{v}}$ are coupling parameters of added mass and J_{comb} is the combined moment of inertia related to CG in z^b-direction.

In Eq. (2), $\boldsymbol{N}(\boldsymbol{\nu})$ is the damping matrix, which is composed only of linear hydrodynamic damping terms $\boldsymbol{N}(\boldsymbol{\nu}) = diag\{-X_u, -Y_v, -N_r\}$, since the vessel is considered moving at low speed.

2.2 Propulsion System

The thrust force F of a propeller can be represented as in Wirtensohn et al. (2015):

$$F = c_1 \rho d_p^4 n|n| - c_2 \rho d_p^3 u_a|n| \tag{6}$$

where n, d_p, ρ, and u_a respectively denote the rotational speed, diameter of the propeller, water density, and rela-

tive speed of the propeller in the axial direction. According to different maneuvers of the vessel, the signs of n and u_a can change, as well as, the values of the parameters c_1 and c_2 in those different scenarios. Therefore, a four-quadrant model is assumed as

$$\begin{pmatrix} c_1 \\ c_2 \end{pmatrix} = \begin{cases} \begin{pmatrix} a_1 & b_1 \end{pmatrix}^T & n \geq 0 \wedge u_a \geq 0 \\ \begin{pmatrix} a_1 & 0 \end{pmatrix}^T & n \geq 0 \wedge u_a < 0 \\ \begin{pmatrix} a_2 & 0 \end{pmatrix}^T & n < 0 \wedge u_a \geq 0 \\ \begin{pmatrix} a_2 & b_2 \end{pmatrix}^T & n < 0 \wedge u_a < 0 \end{cases} \tag{7}$$

This model contains constant parameters a_1, a_2, b_1 and b_2, which were experimentally identified. The axial velocity u_a depends on the body-fixed velocities and is given by $u_a = ucos(\alpha) + (v - rL_{AT})sin(\alpha)$.

While the thrust force of the azimuth thruster (F_{AT}) is given directly by Eq. (6) with $n = n_{AT}$, the force of the bow thruster takes into account the effectiveness of the transverse propulsion by augmenting the thrust force defined in Blanke (1981) by an exponential term Palmer et al. (2008), resulting in the following expression:

$$F_{BT} = c_3 \rho d_p^4 n_{BT} |n_{BT}| e^{-c_b u^2} \tag{8}$$

For the bow thruster, the axial velocity u_a is neglected due to its small value. Hence, the four-quadrant model can be simplified and the value of the constant c_3 will be defined according to the value of n_{BT}.

$$c_3 = \begin{cases} d_1 & n_{BT} \geq 0 \\ d_2 & n_{BT} < 0 \end{cases} \tag{9}$$

where d_1, d_2 and c_b are non dimensional parameters experimentally identified.

The forces and moments that act on the vessel at low speed presented in Eq. (2) are given according to the geometric relations observed in the Fig. 2 as

$$\boldsymbol{\tau}(n_{AT}, \alpha, n_{BT}) = \begin{pmatrix} F_{AT}\cos(\alpha) \\ F_{AT}\sin(\alpha) + F_{BT} \\ F_{BT}L_{BT} - F_{AT}\sin(\alpha)L_{AT} \end{pmatrix} \tag{10}$$

where L_{AT} and L_{BT} are the distances from the origin of the body-fixed frame to the position of azimuth and bow thrusters respectively. The desired forces are achieved by choosing suitable trusters' velocities (n_{AT} and n_{BT}) and orientation angle α. In this case, the thruster allocation problem is incorporated as part of the optimal control problem in order to perform the trajectory tracking. Therefore, the following physical constraints of the thrusters are considered in Section 3:

$$\begin{aligned} & n_{\mathrm{ATMin}} \leq n_{AT} \leq n_{\mathrm{ATMax}} \\ & n_{\mathrm{BTMin}} \leq n_{BT} \leq n_{\mathrm{BTMax}} \\ & |\dot{\alpha}| \leq \dot{\alpha}_{\mathrm{Max}} \end{aligned} \tag{11}$$

where n_{ATMax}, n_{BTMax}, n_{ATMin}, n_{BTMin}, and $\dot{\alpha}_{\mathrm{Max}}$ denote the upper and lower bounds for azimuth thruster's velocity, bow thruster's velocity and azimuth thruster's panning rate respectively.

2.3 Model Identification

The model presented in Sections 2.1 and 2.2 consists of 17 parameters to be identified, where 10 of them are part of the vessel's dynamics ($m, x_g, X_{\dot{u}}, Y_{\dot{v}}, N_{\dot{v}}, Y_{\dot{r}}, J_{comb}, X_u, Y_v, N_r$) and 7 of them are related to the thrusters' forces ($a_1, a_2, b_1, b_2, d_1, d_2, c_b$). The number of unknown parameters can be reduced by assuming that m and x_g are known and that $X_{\dot{u}} = 0.05 \cdot m$ Fossen (1994).

In order to obtain the values of the remaining unknown parameters, the identification algorithm presented in Wirtensohn et al. (2015) was employed. This method estimates all the parameters concurrently and it requires experimental data of the maneuvers performed by the vessel for both identification and validation phases. The identification process consists of solving numerically an optimal problem, using a hybrid approach that combines the particle swarm and interior-point methods. Once the parameters are estimated, a quality analysis based on the Fisher information matrix is performed to evaluate the deviation and correlation of the parameters. At each iteration, the parameter with the greatest deviation above an upper bound γ_r is eliminated and the parameters left are re-identified. When all the parameter deviations are below γ_r, the correlation matrix is analyzed, eliminating the parameter with the highest correlation coefficient, above the correlation upper bound γ_c. The final model is obtained when all the parameters left have their deviation and correlation coefficients below the upper bounds γ_r and γ_c.

The result of the identification process is a not overparameterized model, which is then compared with experimental data sets, validating that the identified model corresponds to the dynamics of the real vessel. It is important to highlight that the data sets used in this validation phase were different from the ones used in the identification phase.

3. CONTROL PROBLEM FORMULATION

In this section, the nonlinear model predictive control (NMPC) scheme is developed to address the trajectory tracking problem for the vessel's dynamic model described in Section 2. It is assumed that all states of the vessel are measured or can be accurately estimated.

3.1 Extended control model

A multivariable integral action is explicitly introduced as in Gehan et al. (2019) to increase the control's design accuracy, leading to the following extended model:

$$\begin{aligned} \dot{\boldsymbol{\eta}} &= \boldsymbol{R}(\psi)\boldsymbol{\nu} \\ \dot{\boldsymbol{\nu}} &= \boldsymbol{M}^{-1}(\boldsymbol{\tau}(n_{AT}, \alpha, n_{BT}) - \boldsymbol{C}_{RB}(\boldsymbol{\nu})\boldsymbol{\nu} - \boldsymbol{N}(\boldsymbol{\nu})\boldsymbol{\nu}) \\ \dot{\boldsymbol{f}} &= \boldsymbol{\mu} + \boldsymbol{\mu}_{FF} \end{aligned} \tag{12}$$

where $\boldsymbol{f}$ is the vector composed of the physical control variables, i.e. n_{AT}, α and n_{BT}, $\boldsymbol{\mu}$ is the new input vector, which corresponds to the first derivatives of $\boldsymbol{f}$ and $\boldsymbol{\mu}_{FF}$ is the feedforward term composed of the reference trajectories of the inputs $\boldsymbol{\mu}$.

3.2 Nonlinear Model Predictive Control Design

Considering the extended control model Eq. (12), the thrusters' physical constraints Eq. (11) and the desired reference state trajectories ($\boldsymbol{\eta}_d, \boldsymbol{\nu}_d, \boldsymbol{f}_d$), generated by a

virtual vessel with the same dynamics, the optimal control problem can be formulated as:

$$\min_{\boldsymbol{\mu}} \; J(\boldsymbol{\eta},\boldsymbol{\nu},\boldsymbol{u},\boldsymbol{\mu}) = \min_{\boldsymbol{\mu}} \int_0^T \|\boldsymbol{\eta}-\boldsymbol{\eta}_d\|^2_{Q_\eta} + \|\boldsymbol{\nu}-\boldsymbol{\nu}_d\|^2_{Q_\nu} + \|\boldsymbol{f}-\boldsymbol{f}_d\|^2_{R_f} + \|\boldsymbol{\mu}\|^2_{R_\mu}\, dt \tag{13}$$

subject to

$$\dot{\boldsymbol{\eta}} = \boldsymbol{R}(\psi)\boldsymbol{\nu} \tag{14a}$$

$$\dot{\boldsymbol{\nu}} = \boldsymbol{M}^{-1}(\boldsymbol{\tau}(n_{AT},\alpha,n_{BT}) - \boldsymbol{C}_{RB}(\boldsymbol{\nu})\boldsymbol{\nu} - \boldsymbol{N}(\boldsymbol{\nu})\boldsymbol{\nu}) \tag{14b}$$

$$\dot{\boldsymbol{f}} = \boldsymbol{\mu} + \boldsymbol{\mu}_{FF} \tag{14c}$$

$$n_{\mathrm{ATMin}} \leq n_{AT} \leq n_{\mathrm{ATMax}} \tag{14d}$$

$$n_{\mathrm{BTMin}} \leq n_{BT} \leq n_{\mathrm{BTMax}} \tag{14e}$$

$$\boldsymbol{\mu}_{\mathbf{Min}} \leq \boldsymbol{\mu} \leq \boldsymbol{\mu}_{\mathbf{Max}} \tag{14f}$$

$$|\boldsymbol{\mu}_{\mathrm{current}} - \boldsymbol{\mu}_{\mathrm{previous}}| \leq \boldsymbol{\Delta\mu}_{\mathbf{Max}} \tag{14g}$$

where the cost function Eq. (13) is minimized, over a finite prediction horizon T, with respect to $\boldsymbol{\mu}$ subjected to the dynamic model constraints Eq. (14a), Eq. (14b), Eq. (14c), the physical constraints of the thrusters Eq. (14d), Eq. (14e) and constraints to limit the inputs and its variations Eq. (14f) and Eq.(14g) respectively. Usually, as in Lutz and Meurer (2021), there is no established boundary between the input values from one step of NMPC to another, allowing possible wide variations in the input values. Hence, the constraint Eq. (14g) was added to restraint this variation to a maximum value given by $\boldsymbol{\Delta\mu}_{\mathbf{Max}}$. $\boldsymbol{Q}_{\boldsymbol{\eta}}$, $\boldsymbol{Q}_{\boldsymbol{\nu}}$, $\boldsymbol{R}_{\boldsymbol{f}}$ and $\boldsymbol{R}_{\boldsymbol{\mu}}$ are positive definite weighting matrices that penalize the deviations from the desired trajectories.

4. SIMULATION AND RESULTS

4.1 Results of Parameter Identification

In order to accomplish an accurate trajectory tracking, a reliable model of the vessel's dynamic behavior is needed. Therefore, all the unknown parameters of the model presented in Section 2.3 were obtained experimentally at the lake Constance in Germany using Solgenia, illustrated in Figure 1, which is equipped with 3-axis automotive inertial measurement unit (IMU) and two antenna Trimble (BX982) RTK-GPS system with 0.1m position accuracy and 0.1° accuracy for the yaw angle.

The data for the identification process was collected under suitable conditions, i.e. the effects of disturbances (current, waves and wind) were low and Solgenia performed a set of maneuvers to obtain a rich range of data sets to achieve an accurate parameter identification. After the collection phase, all the data were smoothed using a Fixed-Point Kalman Smoother as presented in Chowdhary and Johnson (2011) and they were separated into two groups, one was formed by 17 data sets used in the identification process described in Section 2.3, and the other one was formed by 9 data sets for the validation of the dynamic model found.

The values obtained from the identification process are shown in Table 1. As it can be observed, the parameters b_1, b_2 and c_b were eliminated during the evaluation phase as explained in Section 2.3. Therefore, the propulsion system can be represented only using the parameters a_1, a_2, d_1, d_2.

Table 1. Hydrodynamic Identified Parameters.

m	3100kg	X_u	$-86.5\frac{\mathrm{N}}{\mathrm{m/s}}$	a_1	0.9047
x_g	0m	Y_v	$-796\frac{\mathrm{N}}{\mathrm{m/s}}$	a_2	0.6545
$X_{\dot{u}}$	−155kg	N_v	$-958\frac{\mathrm{N}}{\mathrm{m/s}}$	d_1	0.0461
$Y_{\dot{v}}$	−1070kg	N_r	$-5230\frac{\mathrm{N}}{\mathrm{m/s}}$	d_2	0.0548
$N_{\dot{v}}$	−3328kg	Y_r	$-896\frac{\mathrm{N}}{\mathrm{m/s}}$		
$Y_{\dot{r}}$	−1008kg				
J_{comb}	21179kgm^2				

The validation of the identified model consists of evaluating the root mean square error (RMSE) obtained from a comparison between the body-fixed velocities from the experimental data sets, with the ones generated by the identified model in simulation using the same input values shown in Figure 3. This comparison for a docking maneuver is illustrated in Figure 4, and it can be observed that the RMSE values for all body-fixed velocities are of the order 10^{-2}, indicating that the identified model is accurate enough to simulate the real vessel's dynamics.

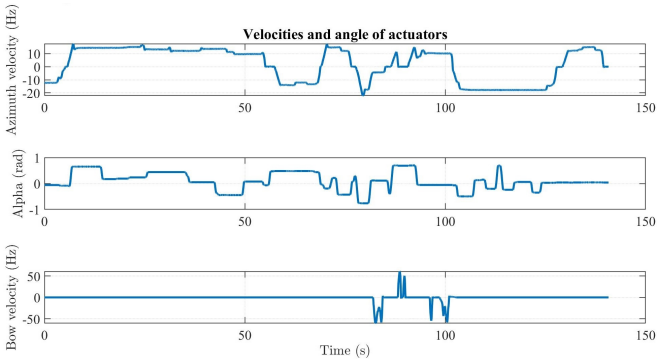

Fig. 3. Input values applied to the identified model.

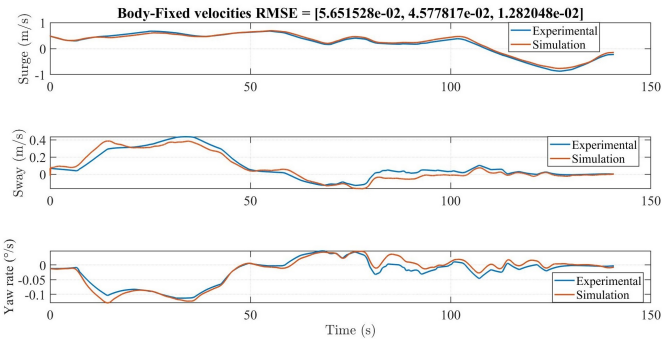

Fig. 4. Comparison of body-fixed velocities from simulated model and experimental validation data set for a docking maneuver.

4.2 Trajectory Tracking Simulation Results

Once the identified dynamic model of Solgenia was obtained, it was used to build a simulator of the vessel to generate the reference trajectories for the states and inputs. An evaluation of the performance of the proposed NMPC controller is realized in simulation using the GRAMPC framework Englert et al. (2019) and MATLAB.

For this work, a curved trajectory was chosen as reference and it was generated by applying $n_{AT}(t) = 3\text{Hz}$, $n_{BT}(t) = 0\text{Hz}$ and $\alpha(t) = 2.4528 \times 10^{-4} t$ rad, where t is the simulation time sampled with $\Delta t = 1s$. The initial reference conditions used were $x_r(0) = 100\text{m}$, $y_r(0) = 200\text{m}$, $\psi_r(0) = 0\text{rad}$, $u_r(0) = 0\text{m/s}$, $v_r(0) = 0\text{m/s}$, $r_r(0) = 0\text{rad/s}$, $n_{AT}(0) = 3\text{Hz}$, $\alpha(0) = 0\text{rad}$, and $n_{BT}(0) = 0\text{Hz}$. Besides that, a step disturbance was added at the states $\boldsymbol{f}$ of the system, being defined as $\delta = [10, 0, 0]^T$ for $t \geq 800s$ and $\delta = [0, 0, 0]^T$ otherwise, generating an abrupt input variation that could represent a force pushing the vessel. The simulations were made by adjusting the NMPC parameters separately to assess its impact on the controller's performance, but they all shared the same initial conditions and reference trajectories.

Prediction Horizon Its impact on the trajectory tracking performance was studied by simulation results as shown in Figure 5. For these first results, the constraints were inactive and the weighting matrices chosen were: $\boldsymbol{Q_\eta} = diag(1.0, 1.0, 30.0)$, $\boldsymbol{Q_\nu} = diag(1.0, 1.0, 1.0)$, $\boldsymbol{R_f} = diag(1.0, 1.0, 1.0)$ and $\boldsymbol{R_\mu} = diag(1.0, 1.0, 1.0)$.

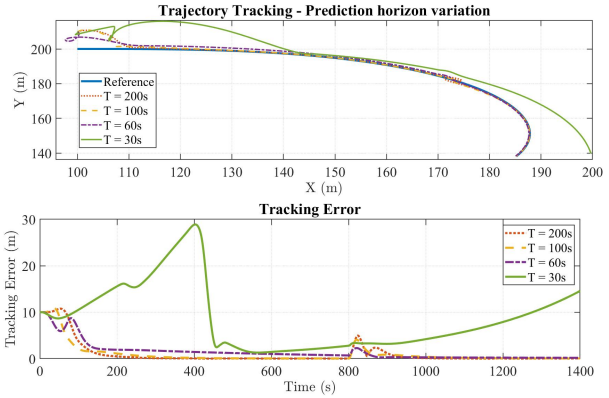

Fig. 5. Simulation results with prediction horizon variation.

From Figure 5, it is clear that the longer is the prediction horizon, the faster and more accurate is the tracking performance of the controller since it has small tracking errors, and it has rejected the input disturbance. The only exception is $T = 30s$, where the controller exhibits an unstable control behavior. For $T = 60s$, the trajectory presents a loop at the beginning, due to the trajectory tracking characteristic, which makes the controller calculate the closest position possible from the reference at each given time instant causing the loop maneuver.

Weighting Matrices These are also important parameters that need to be tuned to obtain a more suitable performance from the controller in a closed-loop. Their influence can be observed by choosing the unstable case shown in Figure 5 ($T = 30s$). The most relevant results were obtained when the weighting matrices were $\boldsymbol{Q_\eta} = diag(300.0, 3000.0, 100000.0)$, $\boldsymbol{Q_\nu} = diag(1.0, 1.0, 1.0)$, $\boldsymbol{R_f} = diag(50.0, 50.0, 1.0)$, $\boldsymbol{R_\mu} = diag(50.0, 50.0, 1.0)$. Figure 6 shows that, with the values found for the weighting matrices, the controller is capable of achieving a stable behavior with a tracking error of $1m$, demonstrating the controller's high sensitivity to the weighting matrices tuning process. Besides that, with the new weighting values, the controller is also able to reject the input disturbance as shown in Figure 7.

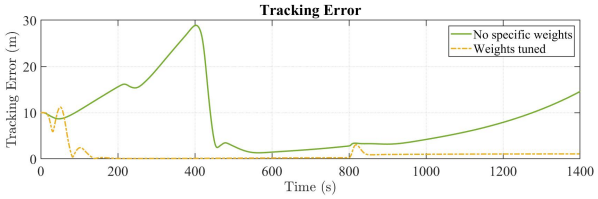

Fig. 6. Tracking error results tuning weighting matrices with $T = 30s$.

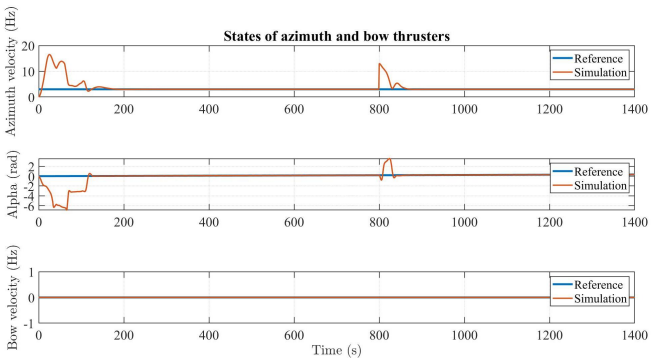

Fig. 7. Input disturbances rejection at the states representing the propellers' velocities and angle for $T = 30s$.

Constraints' effects Besides the calibration of NMPC parameters, the constraints also have a decisive impact on the controller's performance. Using $T = 30s$ and the weighting matrices previously found, the outcome of tightening the state constraint Eq. (14d) was analyzed as shown in Figure 8. As it can be observed, even if the tracking error increases as the constraint values get tighter, the controller is still stable and capable of rejecting the input disturbance. Therefore, its performance could be improved, for instance, by changing the weighting matrices values.

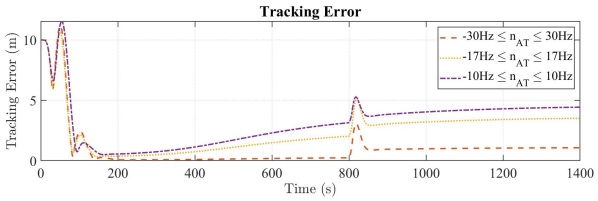

Fig. 8. Tracking error results varying state constraint.

A similar behavior can be observed in Figure 9 with the input constraints Eq. (14f) variation. The controller is capable of rejecting the input disturbance, but the tracking error has increased until it remains around $3m$. The constraint represented in eq. (14g) is responsible for restraining the input's variation from one NMPC step to another. The effects of activating these constraints can be observed in Figure 10. In the same way as the other constraints, the tracking error has increased as the constraints have tightened. However, the variation of the tracking error was not significant over time as the values obtained with the input constraints, showing that the trajectory does not require fast derivations of the inputs.

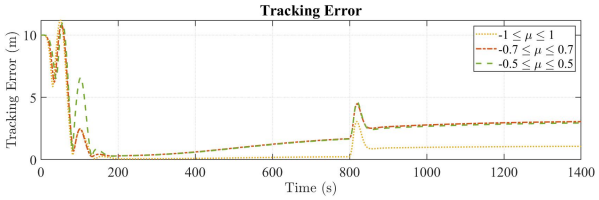

Fig. 9. Tracking error results varying inputs constraints.

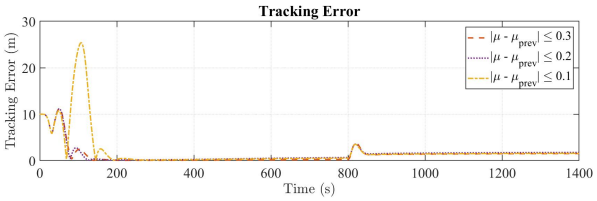

Fig. 10. Tracking error results varying input increment constraints.

5. CONCLUSION

In this paper, a constrained NMPC approach combined with a multivariable integral action was presented to address the trajectory tracking problem. The unknown model parameters were identified and validated using experimental data of various maneuvers of the vessel Solgenia. An evaluation of the controller's performance was made, varying the prediction horizon, weighting matrices and tightening state, input and input increment constraints, showing that the controller presents a high sensitivity to the weighting matrices values and it can respect the constraints when these are not too restricted. In the future, the controller design will consider not only constraints to allow the vessel to perform a docking maneuver but also environmental disturbances for real-time implementation on the Solgenia.

REFERENCES

Abdelaal, M. and Hahn, A. (2016). NMPC-based trajectory tracking and collision avoidance of unmanned surface vessels with rule-based colregs confinement. In *2016 IEEE Conference on Systems, Process and Control (ICSPC)*, 23–28.

Blanke, M. (1981). *Ship Propulsion Losses Related to Automatic Steering and Prime Mover Control*. Technical University of Denmark.

Chowdhary, G. and Johnson, E. (2011). Theory and flight-test validation of a concurrent-learning adaptive controller. *Journal of Guidance Control and Dynamics*, 34, 592–607.

COLREGS (1972). International regulations for preventing collisions at sea. *Convention on the International Regulations for Preventing Collisions at Sea*, pp. 1–74.

Dai, Y., Yang, C., Yu, S., Mao, Y., and Zhao, Y. (2019). Finite-time trajectory tracking for marine vessel by nonsingular backstepping controller with unknown external disturbance. *IEEE Access*, 7, 165897–165907.

Englert, T., Völz, A., Mesmer, F., Rhein, S., and Graichen, K. (2019). A software framework for embedded nonlinear model predictive control using a gradient-based augmented lagrangian approach (GRAMPC). *Optimization and Engineering*, 20, 769–809.

Fossen, T. (1994). *Guidance and Control of Ocean Vehicles*. Wiley.

Fossen, T. (2011). *Handbook of Marine Craft Hydrodynamics and Motion Control*. Wiley.

Gehan, O., Pigeon, E., Menard, T., Mosrati, R., Pouliquen, M., Fall, L., and Reuter, J. (2019). Dissolved oxygen level output feedback control based on discrete-time measurements during a pseudomonas putida mt-2 fermentation. *Journal of Process Control*, 79, 29–40.

Hagen, I.B., Kufoalor, D.K.M., Brekke, E.F., and Johansen, T.A. (2018). MPC-based collision avoidance strategy for existing marine vessel guidance systems. In *2018 IEEE International Conference on Robotics and Automation (ICRA)*, 7618–7623.

Liu, C., Zou, Z., and Yin, J. (2015a). Trajectory tracking of underactuated surface vessels based on neural network and hierarchical sliding mode. *Journal of Marine Science and Technology*, 20, 322–330.

Liu, C., Zheng, H., Negenborn, R.R., Chu, X., and Wang, L. (2015b). Trajectory tracking control for underactuated surface vessels based on nonlinear model predictive control. In F. Corman, S. Voß, and R.R. Negenborn (eds.), *Computational Logistics*, 166–180. Springer International Publishing.

Liu, Z., Zhang, Y., Yu, X., and Yuan, C. (2016). Unmanned surface vehicles: An overview of developments and challenges. *Annual Reviews in Control*, 41, 71 – 93.

Lutz, M. and Meurer, T. (2021). Optimal trajectory planning and model predictive control of underactuated marine surface vessels using a flatness-based approach. *ArXiv*, abs/2101.12730.

Palmer, A., Hearn, G., and Stevenson, P. (2008). Modelling tunnel thrusters for autonomous underwater vehicles. In *Navigation, Guidance and Control of Underwater Vehicles (NGCUV'08) (10/04/08)*.

Wang, W., Mateos, L.A., Park, S., Leoni, P., Gheneti, B., Duarte, F., Ratti, C., and Rus, D. (2018). Design, modeling, and nonlinear model predictive tracking control of a novel autonomous surface vehicle. In *2018 IEEE International Conference on Robotics and Automation (ICRA)*, 6189–6196.

Wang, W., Shan, T., Leoni, P., Fernández-Gutiérrez, D., Meyers, D., Ratti, C., and Rus, D. (2020). Roboat II: A novel autonomous surface vessel for urban environments. *ArXiv*, abs/2007.10220.

Wen, G., Ge, S.S., Chen, C.L.P., Tu, F., and Wang, S. (2019). Adaptive tracking control of surface vessel using optimized backstepping technique. *IEEE Transactions on Cybernetics*, 49, 3420–3431.

Wirtensohn, S., Wenzl, H., Tietz, T., and Reuter, J. (2015). Parameter identification and validation analysis for a small USV. In *2015 20th International Conference on Methods and Models in Automation and Robotics (MMAR)*, 701–706.

Yan, Z. and Wang, J. (2012). Model predictive control for tracking of underactuated vessels based on recurrent neural networks. *IEEE Journal of Oceanic Engineering*, 37, 717–726.

Zheng, H., Negenborn, R.R., and Lodewijks, G. (2014). Trajectory tracking of autonomous vessels using model predictive control. *IFAC Proceedings Volumes*, 47, 8812 – 8818.